Assessing Snowfall Rates from X-Band Radar Reflectivity Measurements

SERGEY Y. MATROSOV

Cooperative Institute for Research in Environmental Sciences, University of Colorado, and NOAA/Earth System Research Laboratory, Boulder, Colorado

CARROLL CAMPBELL

NOAA/Earth System Research Laboratory, Boulder, Colorado

DAVID KINGSMILL AND ELLEN SUKOVICH

Cooperative Institute for Research in Environmental Sciences, University of Colorado, and NOAA/Earth System Research Laboratory, Boulder, Colorado

(Manuscript received 30 September 2008, in final form 1 July 2009)

ABSTRACT

Realistic aggregate snowflake models and experimental snowflake size distribution parameters are used to derive X-band power-law relations between the equivalent radar reflectivity factor Z_e and the liquid equivalent snowfall precipitation rate S ($Z_e = AS^B$). There is significant variability in coefficients of these relations caused by uncertainties in the snowflake bulk densities (as defined by the mass–size relationships), fall velocities, and particle size distribution parameters. The variability in snowflake parameters results in differing Z_e–S relations that provide more than a factor of 2 difference in precipitation rate and liquid equivalent accumulation estimates for typical reflectivity values observed in snowfall (~20–30 dBZ). Characteristic values of the exponent B in the derived for dry snowfall relations were generally in the range 1.3–1.55 (when Z_e is in mm^6 m^{-3} and S is in mm h^{-1}). The coefficient A exhibited stronger variability and varied in the range from about 30 (for aircraft-based size distributions and smaller density particles) to about 140 (for surface-based size distributions). The non-Rayleigh scattering effects at X band result in diminishing of both A and B, as compared to the relations for longer wavelength radars. The snowflake shape and orientation also influences its backscatter properties, but to a lesser extent compared to the particle bulk density. The derived relations were primarily obtained for snowfall consisting of dry aggregate snowflakes. They were applied to the X-band radar measurements during observations of wintertime storms. For approximately collocated measurements, the in situ estimates of snowfall accumulations were generally within the range of radar-derived values when the coefficient A was around 100–120.

1. Introduction

Meteorological radars that operate at X-band frequencies (wavelength $\lambda \sim 3$ cm) have recently gained considerable interest as a tool for high-resolution rainfall measurements at relatively short distances (typically less than 40–50 km; e.g., Matrosov et al. 2005b; Brotzge et al. 2006). This interest and the associated progress in using X-band radars in quasi-operational observations owes, in part, to the introduction of polarimetric schemes for reflectivity and differential reflectivity corrections of X-band radar signals in rain (e.g., Matrosov et al. 2002; Anagnostou et al. 2004; Park et al. 2005). To a significant degree, such schemes helped to overcome rain attenuation effects, which in the past presented a major limitation for the use of X-band frequency radars for precipitation studies.

Over the last several years, the National Oceanic and Atmospheric Administration (NOAA) Earth System Research Laboratory (ESRL) deployed its transportable polarimetric scanning X-band radar for hydrological studies (HYDROX) in the western slopes of California's Sierra Nevada. This radar has been recently upgraded with a new data system and is capable of high-resolution precipitation mapping (e.g., Matrosov et al. 2007). The HYDROX deployments were part of the Hydrometeorological Test

Corresponding author address: Sergey Y. Matrosov, R/PSD2, 325 Broadway, Boulder, CO 80305.
E-mail: sergey.matrosov@noaa.gov

DOI: 10.1175/2009JTECHA1238.1

Bed (HMT) project, which is aimed at the detailed studies of wintertime storms that are crucial for California's water supply. These deployments took place in the north fork of the American River basin (ARB). Depending on the temperature of a particular weather system, wintertime storms in this basin vary from all rainfall to all snowfall conditions.

Most of the recent attention in X-band radar hydrometeorological applications was generally paid to rainfall studies, and snowfall measurements using radars operating at this frequency were not studied extensively. However, they are also quite important given the increased use of X-band radars in colder conditions. With appropriate retrieval algorithms, radar measurements can be used to obtain spatial snowfall rate patterns and liquid equivalent snow accumulations maps over large areas, thus providing valuable hydrological information.

Radar snowfall measurements present some additional challenges compared to rainfall measurements. These challenges are primarily associated with larger uncertainties in snowflake densities, shapes, orientations, and fall velocities compared to those of raindrops. The attenuation of radar signals is also a significant issue for wet snow observations. In wet snow, attenuation usually exceeds that for rain with comparable precipitation rates (Matrosov 2008), but attenuation in dry snow, which is observed at temperatures below freezing, is generally very small and is usually ignored for many practical cases. Although there is no unambiguous and widely adopted definition of dry snow, observationally based criteria for such snow may be helpful. As was shown, for example, by Ryzhkov et al. (2005), dry falling snow, which primarily consists of aggregates, is characterized by reflectivities that are mostly in a range between 20 and 35 dBZ and differential reflectivities that are usually less than about 0.5–0.6 dB. Wet snow (e.g., snowflakes observed in the melting layer) usually exhibits higher reflectivities and differential reflectivities. Snowfalls consisting of single crystals are characterized by lower reflectivities (usually less than 20 dBZ) and high differential reflectivities. Dry snowfalls consisting of aggregate snowflakes are of the main interest in this study. Such snowflakes were observed during the experimental events considered here.

The larger uncertainties in snowflake properties result in significant uncertainties of relations between the radar reflectivity factor Z_e, which is the main radar measurable, and the liquid equivalent snowfall precipitation rate S. Such relations for rainfall and snowfall present the basis for traditional radar-based quantitative precipitation estimations (QPE), and they generally exhibit more variability for snowfall than for rainfall. Although polarimetric radar observations of depolarization ratios have been shown to provide information on ice/snow hydrometeor habits (e.g., Matrosov et al. 2001), and differential reflectivity measurements can help to distinguish between dry and wet snow, the polarimetric data are quite difficult to interpret quantitatively in terms of snowfall precipitation rate (compared to polarization radar measurements of rainfall rate), so snowfall QPE measurements rely mostly on radar reflectivity data.

Although a dual-wavelength radar approach offers a promise of more accurate retrievals (e.g., Matrosov 1998), collocated radar measurements at a shorter wavelength are often unavailable in operational settings. This study employs a modeling approach to derive X-band radar Z_e–S relations for dry snowfall. Similar approaches have been used in the past for longer wavelengths where the Rayleigh scattering is generally valid (e.g., Rasmussen et al. 2003). A set of assumptions about snowflake properties covering the observed range of these properties and experimental snowflake size distributions (SSDs) are used for these derivations. The derived relations are applied to the HYDROX data during dry snowfalls and compared to available in situ estimates of snowfall.

2. Snowflake backscatter properties

Backscatter properties of individual hydrometeors depend on their size, mass, shape, and orientation. Unlike water drops, the relation between mass and size of ice hydrometeors is not unique and varies quite significantly. Traditionally, relations between sizes D and masses m of ice particles are expressed by power-law approximations:

$$m = aD^b, \tag{1}$$

where the coefficients a and b are found from microphysical studies. Relation (1) determines bulk density of snowflakes ρ_s. The ice hydrometeor mass usually increases with size more slowly than the snowflake volume (i.e., $b < 3$), and ρ_s decreases with size.

Figure 1 depicts the aggregate snowflake bulk density as a function of size for several m–D relations. Note that appreciable precipitation rates are usually observed from snowfall consisting of aggregate snowflakes. A spherical snowflake model was assumed (i.e., D is the snowflake diameter in Fig. 1). Shown are aggregate particle bulk densities from Holroyd (1971) and those resulting from m–D relations presented in Matrosov (2007) and Kingsmill et al. (2003). The Kingsmill (2003) relation is based on the data by Heymsfield et al. (2002). These relations are given in cgs units as

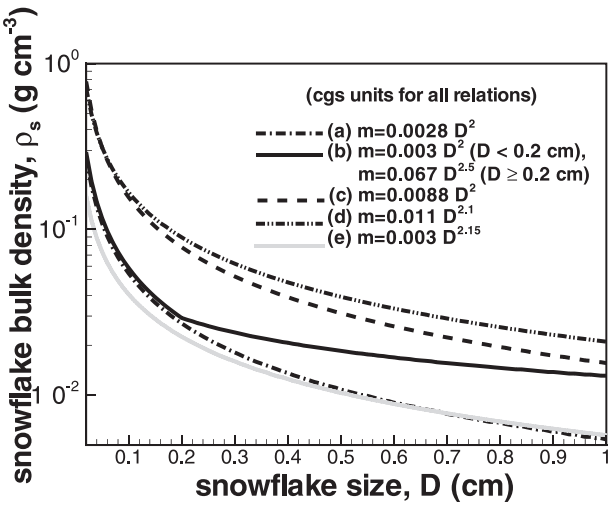

FIG. 1. Aggregate snowflake bulk density as a function of size for several *m–D* relations. Curves (a),(b), and (c) represent *m–D* relations from Eq. (2). Curves (d) and (e) represent *m–D* relations from Brandes et al. (2007) and Mitchell (1996), respectively.

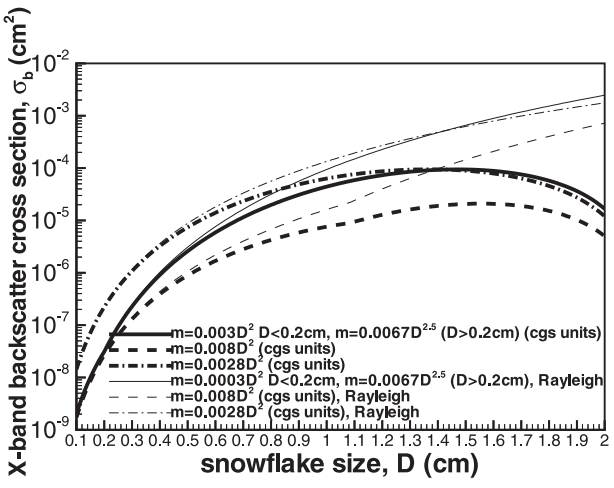

FIG. 2. Snowflake backscatter cross sections as a function of size for different *m–D* relations. Thick lines show results of the T-matrix calculations, and thin lines show results of the Rayleigh approximation.

$$m = 0.0028D^2 \text{ (Kingsmill et al. 2003)}, \tag{2a}$$

$$m = 0.003D^2 (D < 0.2\,\text{cm}), \quad m = 0.067D^{2.5} (D \geq 0.2\,\text{cm}) \times \text{(Matrosov 2007)}, \quad \text{and} \tag{2b}$$

$$m = 0.0088D^2 \text{ [from Holroyd (1971) densities]}. \tag{2c}$$

The results from Holroyd (1971) were found to satisfactorily approximate recent results by Brandes et el. (2007, their Fig. 6; with Holroyd's densities of $\rho_s = 0.017D^{-1}$, with cgs units), though the Brandes et al. (2007) relation (also shown in Fig. 1) overestimates a little the results from (2c). It should be mentioned, however, that observations of warm snowfalls with temperatures close to freezing might have influenced this relation. The relation (2a) is representative for a number of *m–D* relations used in the ice cloud microphysics and remote sensing community, including ones from Brown and Francis (1995) and Mitchell (1996), which is also shown in Fig. 1.

As seen from Fig. 1, for particle sizes up to about 1 mm, the composite *m–D* relation (2b) closely approximates the relation (2a). For larger snowflake sizes, which are observed in heavier snowfalls, relation (2b) provides a continuous transition from densities that are characteristic of smaller aggregates typically found in clouds and weak precipitation, to densities that are more appropriate for larger dry snowflakes near the surface, as documented by Magono and Nakamura (1965, their Fig. 3). Although there are many more experimental *m–D* relations found in the literature, the overall spread of ρ_s values resulting from the choice of the *m–D* relation in Fig. 1 provides a measure of a degree of uncertainty in snow particle bulk densities. This uncertainty is a significant contributor into variability of snowflake backscatter properties.

X-band ($\lambda = 3.2$ cm) backscatter cross sections σ_b of aggregate dry snowflakes as a function of snowflake size are shown in Fig. 2. These cross sections were calculated using the T-matrix method (Barber and Yeh 1975). A dry snowflake was considered a uniform mixture of solid ice and air, and the complex refractive index of this mixture m_s was calculated from

$$(m_s^2 - 1)(m_s^2 + 2)^{-1} = P_i(m_i^2 - 1)(m_i^2 + 2)^{-1}, \tag{3}$$

where m_i is the complex refractive index of solid ice ($m_i \approx 1.78 + i0.0002$ at X band) and P_i is the relative volume of solid ice in a mixture ($P_i \approx \rho_s\rho_i^{-1}$; $\rho_i = 0.916$ g cm^{-3}).

For smaller particles that are within the Rayleigh scattering regime (i.e., $\pi D/\lambda \ll 1$ and $\pi D|m_s|/\lambda \ll 1$), backscatter cross sections are proportional to m^2, so the difference of about a factor of 3 in bulk densities from the *m–D* relations translates to almost one order of magnitude difference in corresponding values of σ_b. It can be seen that the Rayleigh results at X band are generally valid for sizes up to approximately 4–5 mm. For sizes greater than about 1.5 cm, the backscatter cross sections diminish with size because of stronger non-Rayleigh scattering effects. Note that these characteristic sizes (i.e., 4–5 mm and 1.5 cm) depend on the *m–D* assumption relatively little, because it is snowflake physical dimensions and not densities that are primarily responsible for non-Rayleigh scattering (e.g., Matrosov 1998). When snowflake size spectra are known (e.g.,

from sampling using particle measuring system sensors), ice equivalent reflectivity is often estimated as a normalized sum of the squares of individual particle masses. Such an approach is generally valid under the Rayleigh assumption, but it will not be appropriate for X band when snowflakes greater than 4–5 mm are present (then, full-backscatter cross sections should be used during the summation).

Although some microphysical studies (e.g., Brandes et al. 2007) find that snowflake aggregates are mostly spherical on average, other microphysical studies indicate that mean aspect ratios of aggregate particles are about 0.6–0.8 (e.g., Korolev and Isaac 2003). The nonspherical model was also found to be in better agreement with dual-wavelength (X and W bands) radar observations (Matrosov et al. 2005a). To estimate snowflake nonsphericity effects, T-matrix calculations of backscatter cross sections were performed for the spheroidal aggregate snowflake model with aspect ratios r of 0.6 and 0.8. It was assumed that, in the absence of strong horizontal winds and wind shear, nonspherical snowflakes are oriented preferably with their major dimensions in the horizontal plane. Such orientations (with a standard deviation of about 9°) were observed using radar depolarization measurements in dendrite snowflakes (Matrosov et al. 2005c).

The nonspherical particle calculations of horizontal polarization backscatter cross sections at low radar elevation angles ($\alpha \sim 2°$) were performed assuming different particle shapes (i.e., different values of aspect ratio r) but preserving particle mass. These calculations provided results that differ from those in Fig. 2 but not by more than 15% (not shown). It amounts to only a 0.6-dB difference and can be ignored (if reflectivity factor is the main radar parameter of interest) given the much higher backscatter cross section uncertainties that are associated with the choice of a mass–size relation. Assuming nonspherical snowflake tumbling (i.e., the random orientation) rather than preferable horizontal orientation results in even smaller differences between spherical and nonspherical snowflake aggregate models.

Thus, it can be concluded that the spherical model is generally suitable for modeling nonpolarimetric radar properties (e.g., Z_e) of low-density snowflakes at X-band radar frequencies, especially when the deviation from Rayleigh-type scattering is not very profound. It should be mentioned, however, that the spherical model becomes progressively less suitable (especially for vertical viewing at W band) when the radar frequency increases, and it can be not a good choice for describing even radar reflectivities if particles are substantially nonspherical (Matrosov 2007). The spherical assumption also precludes modeling common polarimetric radar parameters such as differential reflectivity, differential phase shift, and copolar correlation coefficient.

3. Z_e–S relations at X band

The equivalent reflectivity factor (referred to simply as reflectivity) is the main quantitative parameter measured by radar. Reflectivity of an ensemble of snowflakes can be calculated by integrating the backscatter cross sections of individual snowflakes over the size distribution $N(D)$:

$$Z_e = \lambda^4 \pi^{-5} |(m_w^2 + 2)/(m_w^2 - 1)|^2 \int_{D_{\min}}^{D_{\max}} \sigma_b(D) N(D)\, dD, \tag{4}$$

where m_w is the complex refractive index of water ($m_w \approx 7.29 + i2.83$ at 0°C and $\lambda = 3.2$ cm), which is customary used for calibration of weather radars (Smith 1984). The values 0.01 and 1.5 cm for $D_{\min}$ and $D_{\max}$, respectively, were further used in this study. Because the smallest observed bulk densities of snowflakes are around 0.005 g cm^{-3} (e.g., Magono and Nakamura 1965), it was assumed that $\rho_s = 0.005$ g cm^{-3}, even if the use of a particular m–D relation resulted in smaller densities. Similarly, the solid ice density was assumed if m–D relations resulted in density values exceeding 0.916 g cm^{-3}.

Different studies (e.g., Gunn and Marshall 1958, Sekhon and Srivastava 1970, Braham 1990, Harimaya et al. 2000) indicate that SSDs can be satisfactorily approximated by an exponential function:

$$N(D) = N_0 \exp(-\Lambda D), \tag{5}$$

where N_0 and Λ are the intercept and slope parameters, respectively. It should be mentioned that Brandes et al. (2007) also fitted SSDs by a gamma function and estimated μ–a shape parameter of this function. There is no consensus in the community, however (e.g., Moisseev and Chandrasekar 2007), of the accuracy of gamma-function μ estimates; thus, exponential distributions were further used in this study. This choice is also justified by the fact that the information in the literature on most experimental SSDs usually is given in terms of the exponential function parameters N_0 and Λ.

The snowfall rate in terms of melted liquid equivalent S is given as

$$S = \rho_w^{-1} \int_{D_{\min}}^{D_{\max}} m(D) v_t(D) N(D)\, dD, \tag{6}$$

where ρ_w is the density of water and v_t is the fall velocity of snowflakes. As in Matrosov (2007), snowflake fall velocities in this study were modeled by the relation

$$v_t\,(\mathrm{cm\ s^{-1}}) \approx 30 + 50[\log_{10}(D) - 2] \quad (\text{for } D > 100\ \mu\mathrm{m}), \tag{7}$$

which approximates the data presented by Mitchell and Heymsfield (2005, their Fig. 5). The expression (7) reflects a diminishing trend of fall velocity increase with size as snowflakes grow larger. This effect was observed in many experimental studies (e.g., Magono and Nakamura 1965). Fall velocity altitude adjustments resulting from changing air density were also introduced in modeled velocity, as described in Matrosov (2007).

Experimental data on SSDs are not as numerous as for raindrop size distributions. One of the comprehensive studies of SSDs at the ground was published by Braham (1990), who reported experimental values of the intercept N_0 and the exponential slope Λ observed in snowfalls that mostly consisted of aggregated snowflakes. One of the most recent aircraft-based SSD parameter datasets that includes values of N_0 and Λ was published by Woods et al. (2008). Both datasets were obtained at temperatures below freezing and are assumed to be representative of dry snowfalls. In the experimental spectra, values of Λ vary approximately from 1 to 6 $\mathrm{mm^{-1}}$ and the values of N_0 generally vary in the range 0.5–500 $\mathrm{mm^{-1}\ l^{-1}}$. It is worthwhile to note that the correlation between N_0 and Λ is usually relatively low. The corresponding correlation coefficient is only 0.16 for the Braham (1990) SSD parameters, and it is 0.48 for the Woods et al. (2008) parameters. Another important issue worth mentioning is that the ranges of variability in Λ and N_0 that we presented correspond well to recent observational data of Brandes et al. (2007), who also estimated these exponential SSD parameters in their Figs. 11 and 12 (except some data points near 0°C that show smaller values of Λ, which are likely to be from wet snow observations).

Equations (4)–(7) were used to calculate corresponding pairs of Z_e and S for experimental SSD mentioned before. Although this study does not use individual size-resolved snow spectra, it utilizes N_0 and Λ parameters obtained by different authors from such spectra. These parameters vary in the representative ranges of their variability. The resulting scatterplots are presented in Fig. 3. For easier reading in this figure, square symbols show only results for the m–D relation (2b), whereas the best-fit power-law Z_e–S fits are drawn for three m–D relations depicted in Fig. 1. It can be seen that the Z_e–S fits for the relation (2b) are framed by those from relations (2a) and (2c) for both sets of experimental SSD parameters. For a given SSD parameter dataset, snowfall rate estimates from best power-law fits derived using the relations (2c) and (2a) differ by about ±30% from their average. It is significantly less than the corresponding differences in bulk

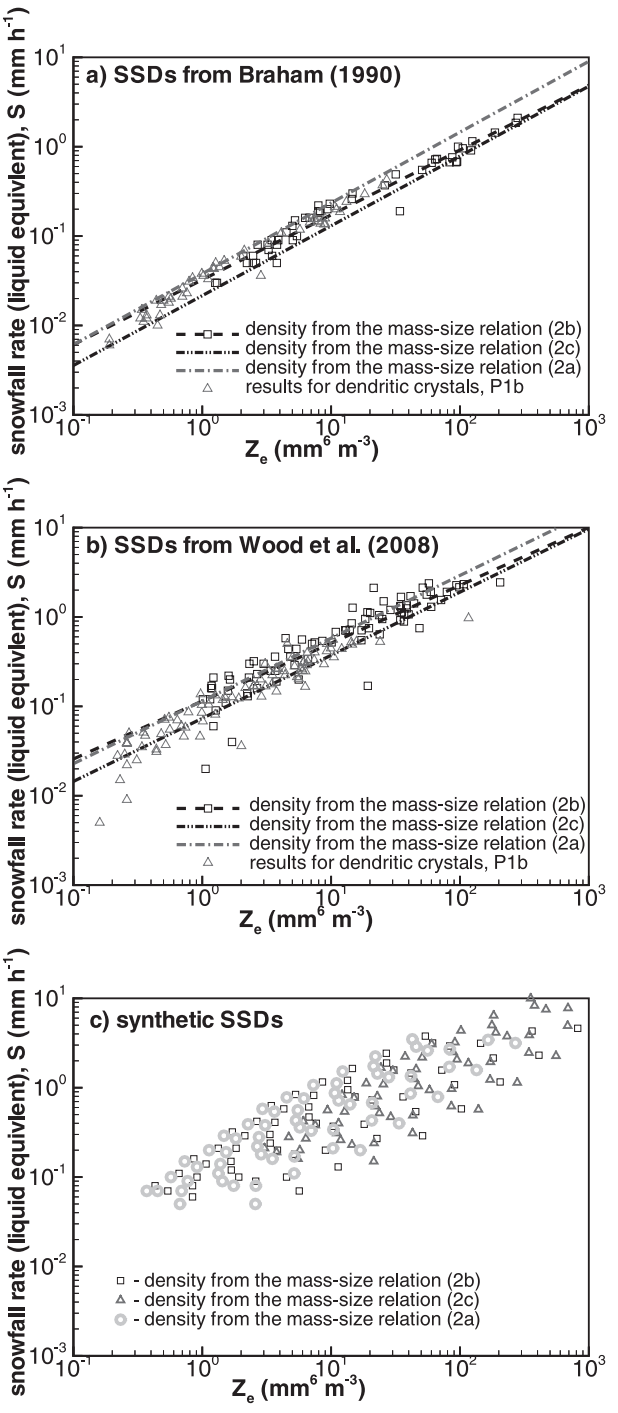

FIG. 3. Reflectivity–snowfall rate power-law relations for different m–D relations and experimental SSDs from (a) Braham (1990) and (b) Woods et al. (2008). Symbols are shown for the m–D relation (2b) (squares) and for dendritic crystals P1b (triangles). (c) Results of modeling with synthetic SSDs and aggregate snowflakes.

TABLE 1. Coefficients in Z_e–AS^B relations (8) shown in Fig. 3.

No.	m–D relation	SSD dataset	A	B
1	(2a)	Braham (1990)	67	1.28
2	(2b)	Braham (1990)	114	1.39
3	(2c)	Braham (1990)	136	1.30
4	(2a)	Woods et al. (2008)	28	1.44
5	(2b)	Woods et al. (2008)	36	1.56
6	(2c)	Woods et al. (2008)	48	1.45

densities (Fig. 1). The reduced sensitivity of the Z_e–S relation power-law fits to the density assumption can be explained by the fact that both Z_e and S increase (decrease) as ρ_s increases (decreases). The reflectivity dependence on density is, however, stronger than that of snowfall rate, so the density increase (decrease) results in shifting the Z_e–S relation fits to the right (left) in Fig. 3.

Table 1 shows the parameters of the Z_e–S relations plotted in Fig. 3. Note that reflectivity was considered as an independent variable when deriving these relations. The parameters A and B presented in Table 1 correspond to the conventional form used in radar meteorology applications,

$$Z_e\ (\mathrm{mm^6\ m^{-3}}) = AS^B\ (\mathrm{mm\ h^{-1}}). \tag{8}$$

Uncertainties in the snowflake fall velocity assumption will result in uncertainties of the coefficients A and B. Increasing (decreasing) v_t values by 30% compared to those predicted by Eq. (7), for example, does not significantly change the coefficient B, but it would cause about a 40% decrease (increase) of the coefficient A. Increasing an assumed value of $D_{\max}$ from 1.5 to 2 cm affects the values of these coefficients relatively minor.

Comparisons of Figs. 3a,b and Table 1 data indicate a significant sensitivity of Z_e–S relations to the SSD parameter dataset choice. It can be seen that there is some data scatter resulting from size distribution details within the same SSD parameter dataset. This data scatter is somewhat greater for the Woods et al. (2008) SSDs than for the Braham (1990) SSDs. Furthermore, the snowfall rates derived from the Z_e–S relations drawn for the same assumption of the bulk density but for different SSD parameter sets [i.e., Braham (1990) SSDs versus Woods et al. (2008) SSDs] can differ by about a factor of 2 for typical snowfall reflectivities (~20–30 dBZ). Given this and assuming independence of uncertainty contributions from the snowflake density and fall velocity assumptions discussed earlier, it can be concluded that overall uncertainty of estimating snowfall rate from radar reflectivity measurements can be as high as a factor of 3 or so.

The data scatter around the best-fit power-law approximations in Figs. 3a,b is relatively modest for both experimental SSD datasets used here. Although the Braham (1990) and Woods et al. (2008) SSD data parameter sets are representative of different snowfalls, the data scatter within these individual datasets may not cover the whole range of variability in Z_e and S. To provide a better perception of a possible spread in Z_e and S values, some synthetic SSDs were generated assuming that Λ and N_0 vary in the ranges mentioned earlier (i.e., 1–6 $\mathrm{mm^{-1}}$ for Λ and 0.5–500 $\mathrm{mm^{-1}\,l^{-1}}$ for N_0). Incremental changes in Λ (by a step of 0.5 $\mathrm{mm^{-1}}$) and in N_0 (by a factor of 2) were used to generate these synthetic SSDs. The corresponding results (after thresholding precipitation rates in a range 0.1 mm $\mathrm{h^{-1}} < S < 10$ mm $\mathrm{h^{-1}}$) are shown in Fig. 3c.

Although such synthetic SSDs modeling can be justified, in part, by the low correlation between Λ and N_0, some unrealistic combination of SSD parameters might not be out of question. Figure 3c, however, provides an illustration of a possible spread in Z_e and S. Comparing Figs. 3a,c and comparing Figs. 3b,c reveals that the data for the Braham (1990) SSDs tend to be in the lower part of the general data spread area, whereas the data for the Woods et al. (2008) SSDs usually correspond to its upper part. Overall, Fig. 3c suggests that, because of SSD details and snowflake densities, the snowfall rates for a given reflectivity may vary as much as a factor of 2–3 relative to the mean value of S for this reflectivity.

Data in Table 1 indicate that, although there is a significant variability in the parameters of Z_e–S relations, a typical value of the exponent B is around 1.4–1.5. The relative variability of the coefficient A is more significant than that for the exponent. Braham (1990) SSDs produce noticeably higher coefficients than those for the Woods et al. (2008) SSDs. The mean values of A around 100–110 are characteristic for the Braham (1990) experimental SSDs and model assumptions considered in this study. The corresponding values of A for the Woods et al. (2008) SSD parameters are only around 40.

Although the choices of the SSD data parameter set and the m–D relation assumptions are two major components to the variability in Z_e–S relations, some temperature dependence in these relations can be expected. The snowfall temperature near the ground in the HMT X-band radar area, however, usually varies little (~−10° to −1°C), so it might be not a significant factor for the current study compared to the other sources of variability. For example, note that, for the same temperature range of −15° to 0°C, the mean temperature stratified relations between ice water content and the Rayleigh reflectivities presented recently by Hogan et al. (2006) and Boudala et al. (2006) differ by a factor of 2–3 at characteristic snowfall values of Z_e in a range of 20–30 dBZ. Because these authors used similar approaches for deriving their

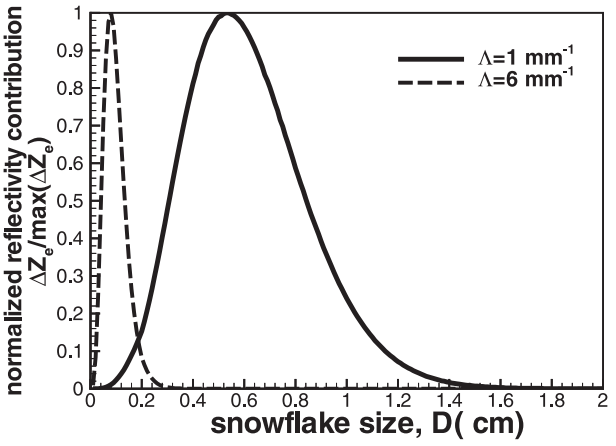

FIG. 4. Normalized contributions of snowflakes of the given size D (± 0.1 mm) to the total reflectivity as a function of snowflake sizes.

relations but different large aircraft crystal datasets and m–D assumptions, it indicates that the dataset issues and mass–size relations might matter more for radar snowfall relations than temperature variations in a relatively narrow interval.

The Z_e–S relations shown in Fig. 3 and Table 1 were derived for dry aggregate snowflakes. Although this type of dry snowfall is common, snowfalls consisting of single crystals can also be observed. The predominant single crystal habit in such snowfalls is usually dendritic (e.g., Matrosov et al. 2001). To assess how well the derived relations can describe the dendritic snowfall, modeling was also performed for the stellar dendritic crystals [P1b, P1c, and P1e, according to the Magono and Lee (1966) classification] and for the same SSDs. The corresponding mass–size and fall velocity–size relations for dendrites were adopted from Mitchell (1996). The dendritic calculation data are also shown in Fig. 3 by triangle symbols. It can be seen that dendritic data generally align with aggregate data well, though their reflectivities and snowfall rates are smaller.

It is useful to estimate the sizes of snowflakes that usually contribute most to snowfall reflectivity. As a function of snowflake size D, Fig. 4 shows the value of the contribution to the total snowfall reflectivity from particles of the given size ($D \pm 0.1$ mm) $\Delta Z_e(D)$, normalized to the maximum of this contribution. The results for the SSD slopes that are close to the minimum and maximum values ($\Lambda = 1\ \text{mm}^{-1}$ and $\Lambda = 6\ \text{mm}^{-1}$) adopted for this study are depicted. Note that values of the intercept parameter N_0 are irrelevant for these results. It can be seen that snowflakes with sizes of about 5–6 mm contribute most in cases of smaller slopes ($1\ \text{mm}^{-1}$), whereas particles of around 1 mm contribute the most for larger slopes ($6\ \text{mm}^{-1}$). Although the presented results correspond to the m–D relation (2b), they generally are representative for other relations too. From results of this figure, one can also obtain (by integrating for corresponding particle size ranges) that particles with $D >$ 1 cm contribute generally less than 7% (0.3 dB) to the total reflectivity even for smallest Λ ($\sim 1\ \text{mm}^{-1}$).

It is instructive to compare the Z_e–S relations derived here with those suggested by different authors in the past. Boucher and Wieler (1985) provided a mean X-band experimental relation for hourly averaged snowfall depth S_s and equivalent radar reflectivity as $Z_e = 5.07S_s^{1.65}$. For the snow-to-liquid ratio of 8:1 (10:1), this relation approximately corresponds to $Z_e \approx 150S^{1.65}$ ($Z_e \approx 220S^{1.65}$). Super and Holroyd (1998) and Hunter and Holroyd (2002) provide experimental Z_e–S relations for different S-band Weather Surveillance Radar-1988 Doppler (WSR-88D) systems. Their values for the coefficient A generally vary between 50 and 200, and a value of B is around 2. At S-band frequencies (wavelengths $\sim$ 10–11 cm), however, the non-Rayleigh scattering effects in snow are much weaker than at X band. To estimate expected S- and X-band differences, modeling calculations using (4) and SSDs employed in this study were also performed for S-band. The results of this modeling indicated that, for snowfall values of Z_e in a range 25–30 dBZ, S-band reflectivities are generally higher than reflectivities at X band by about 1–1.5 dB. Compared to the values in Table 1, S-band values of the coefficient A and the exponent B are usually larger by about 20%–25% and 10%–15%, respectively.

Given the expected S- and X-band differences, it can be concluded that the experimental Z_e–S relations that we mentioned correspond better to the results of this study, which were obtained for Braham's SSD parameters. One reason to this result could be that these SSDs were collected in falling snow at the surface, whereas data of Woods et al. (2008) came from aircraft measurements. The mean experimental relations from the literature sources mentioned earlier may also comprise the data from wider snow conditions (not just dry snowfalls). Compared to dry snow, wetter snow might cause the increase in the coefficient A.

It should be mentioned also that some of the relations between radar parameters and snowfall rate reported in the past are given in terms of the reflectivity values calculated for melted snowflakes under the Rayleigh assumptions (e.g., Z, as in Sekhon and Srivastava 1970). The Rayleigh values of Z are greater than those of Z_e by about 7 dB (Smith 1984), so coefficients A in Z–S relations are significantly larger than those in Z_e–S relations (e.g., $Z = 695S^{2.08}$ for the Rayleigh reflectivity and temperature range between 0 and -15°C; Boudala et al. 2006). As mentioned earlier, the non-Rayleigh

scattering effects at X band decrease the value of the coefficient A even further compared to the case when only the Z_e–Z difference is taken into account.

4. Experimental examples of X-band radar measurements of snowfall

As part of the HMT-08 field project, the NOAA HYDROX was deployed during winter 2007/08 at the Blue Canyon airport (BLU; 39.2707°N, 120.7083°W) at an altitude of 1610 m above mean sea level (MSL) in the Sierra Nevada. The radar was operated only during significant precipitation events and scanned over the North Fork of the ARB. This radar was originally calibrated in the absolute sense using a corner reflector. During each field deployment, the calibration is routinely verified by comparing radar reflectivity measurements in light rain over a nearby disdrometer with reflectivity estimates calculated from the raindrop size distributions from this disdrometer. Disdrometer rainfall accumulation measurements are also verified by comparing to the data from standard rain gauges.

There was a short rain event in the beginning of HMT-08 (which was used for the calibration check). During most of the events in this deployment, snowfalls were observed in the radar coverage area. A simplified classification of snowfalls from the observational radar standpoint (e.g., Ryzhkov et al. 2005) differentiates among wet snowfalls; dry snowfalls consisting mostly of aggregate snowflakes; and snowfalls that consist mainly of pristine ice crystals, which are usually observed at colder temperatures (less than about −5° to −10°C). The majority of HMT-08 observations were in wet snowfall, corresponding to the melting layer conditions in the vicinity of the radar site. Wet snow was accumulating on the antenna, thus degrading the radar performance. Such observational cases were not considered in this study.

Only few brief periods of dry snowfall with aggregate snowflakes in the radar area were observed over the course of the HMT-08 deployment. During these periods, temperatures near the ground were below freezing and decreased with height, with vertical gradients of about −5° to −5.5°C km^{-1} (as inferred from radiosonde soundings). Such dry snow generally did not degrade the performance of the radar, and it was the main interest of this study.

a. An event on 3–4 January 2008

A dry snowfall event observed by the HYDROX from 2315 UTC 3 January to 0120 UTC 4 January 2008 at the BLU site presents a convenient dataset of radar and supporting surface data to assess applicability of the Z_e–S relations discussed earlier. The radar operator during this event observed dry aggregate snowflakes with sizes occasionally reaching up to about 1 cm. The BLU surface meteorology site, which was equipped with tipping-bucket and hot-plate precipitation sensors (Rasmussen et al. 2005), was located at a distance of approximately 600 m north of the radar. The air temperature at the surface near the radar was around −1°C over the course of the event, and it was decreasing with height. No temperature inversions were evident from radiosonde profiles. The ground observations of snow particles did not reveal any significant amount of riming.

The radar setup and nearby trees prevented scanning directly over the BLU site, though the close proximity of this site to the radar allowed the use of its data for comparisons with radar-derived snowfall parameters. The routine radar scanning procedure included sector scan measurements (with 150 m gate sampling) between the azimuthal directions of 60° and 240° at several beam elevation angles between 2° and 5.5°, and a number of range–height indicator (RHI) scans. Although the lower part of the basin could be observed by the radar in an unobstructed way with a beam elevation angle of 1.9°, the view of its upper part east and southeast of the BLU site was obstructed by nearby mountains. A relatively high elevation angle of 5.5° was required to clear these obstacles.

An example of the real-time reflectivity display observed at 0003:35 UTC for the lowest elevation (~1.9°) sector scan during this event is shown in Fig. 5. The North Fork of the ARB is outlined in this figure. It can be seen that snowfall with relatively uniform reflectivity covered unobstructed areas of the basin. The radar beam was in snow for all radar ranges, though sleet and rain conditions were observed at the ground at the surface meteorology sites located in the lower part of the basin, which was observed by the radar at azimuths between about 180° and 240°.

Time series of HYDROX horizontal polarization reflectivity Z_e, differential reflectivity Z_{DR}, and the copolar correlation coefficient ρ_{hv} measurements during the considered event are presented in Fig. 6. The data are shown for the locations centered at approximately 800 m to the southwest and southeast of the radar site (from the lowest elevation sector scans) and also directly over the radar. The lowest ''good'' range gate (where the receiver was out of saturation) vertical measurements were extracted from the RHI radar scans. It can be seen that, although some variability is present, the different curves in Fig. 6 generally follow each other. It indicates that the radar measurements in the vicinity of the BLU site (even though data exactly over this site were not available) might be representative of the area with characteristic dimensions of about ~0.8–1 km around this site.

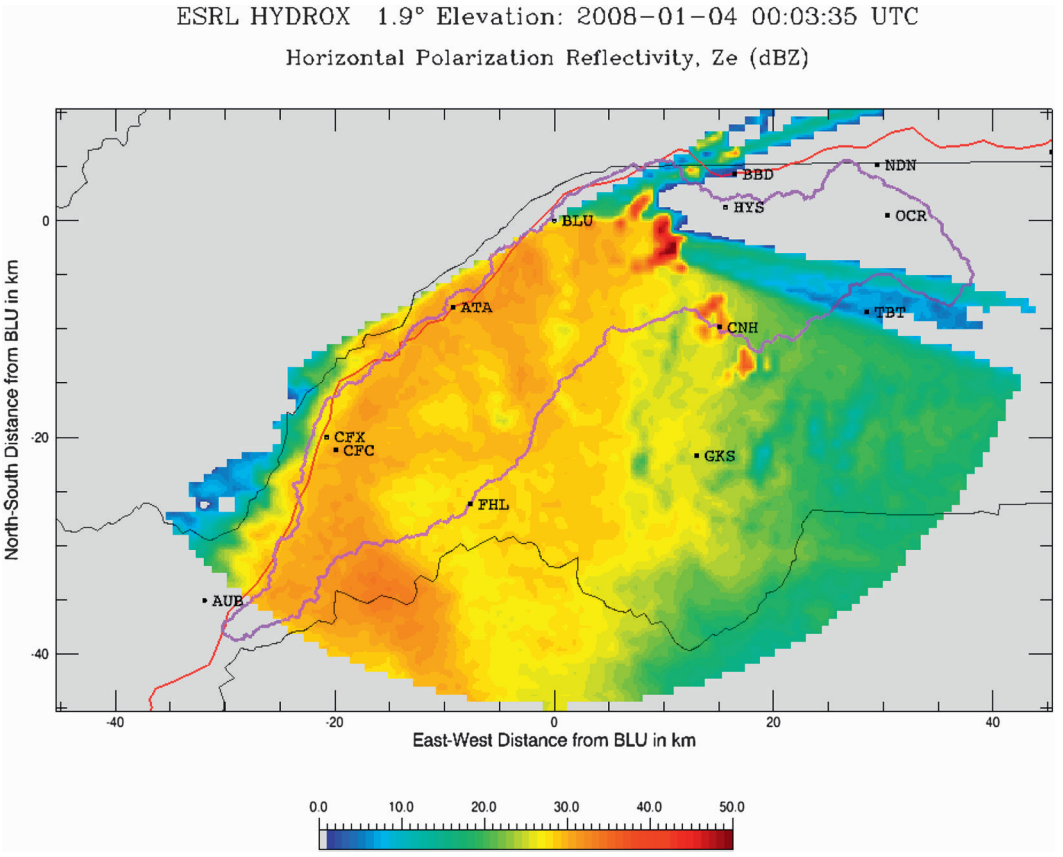

FIG. 5. A display of the horizontal polarization reflectivity Z_e in dB observed by the HYDROX at 0003:35 UTC 4 Jan 2008. The North Fork of the ARB is outlined by a purple line.

The polarimetric capability of the HYDROX provides a means for differentiating among single crystals and dry and wet aggregate snow conditions. The range of observed reflectivity and differential reflectivity in Fig. 6 falls approximately in the middle of the dry snow area in the Z_e–Z_{DR} scatterplot provided by Ryzhkov et al. (2005, their Fig. 8). This area is centered at about 27 dBZ (for Z_e) and 0.2 dB (for Z_{DR}) and extends to

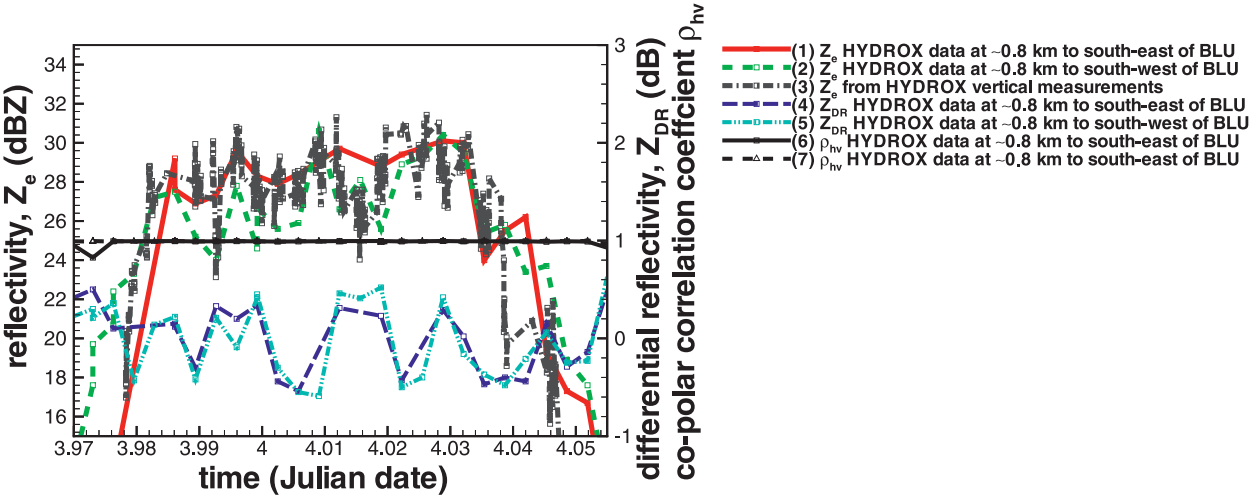

FIG. 6. HYDROX measurements from 2315 UTC 3 Jan to 0120 UTC 4 Jan 2008 in the vicinity of the BLU site.

about ±7 dBZ (for Z_e) and ±0.5 dB (for Z_{DR}) from the center values. It indirectly confirms that observed snow was dry. Note also that, although these ranges of radar parameters were derived for S-band frequencies, they should be approximately valid for X-band measurements as well, because modeling described in section 3 indicates that, for typical snowfall conditions, S-band reflectivities are expected to be greater than those at X band by only 1–1.5 dB and differential reflectivity differences are expected to be within a few tenths of 1 dB. An additional indication that the snow was dry is provided by the ρ_{hv} measurements, which were generally higher than about 0.96–0.97. Wet snow (e.g., measurements in the melting layer) exhibits significantly lower values of ρ_{hv} (e.g., Matrosov et al. 2007).

Snowfall accumulation time series for the event of 3–4 January 2008, as calculated from the HYDROX data using different Z_e–S relations from Table 1, are shown in Fig. 7a. The radar data in this figure correspond to vertical beams, although the use of data from low-elevation scanning in the vicinity of the radar site does not change the results by more than about 15% compared to those in Fig. 7a. Also shown in this figure is the accumulation curve calculated from the hot-plate total precipitation measuring system deployed at the BLU site. At different times, the shape of the hot-plate accumulation curve generally follows the curve shapes for different radar estimators. This might suggest SSD changes over the course of the event.

Although the hot plate recorded about 7.8 mm of total liquid equivalent for the event, the different Z_e–S power-law relations provided accumulations in a range from 5 to 15 mm. The results from the relations that use m–D approximations from (2b) and (2c) are quite close, because these relations yield similar snowfall rate values for reflectivities in the range of 26–30 dBZ, which were typical for this event (Fig. 3). The Z_e–S relations derived with the use of the aforementioned m–D approximations and Braham (1990) SSDs underestimate the hot-plate measurement by about 2 mm, and the ones obtained with the Woods et al. (2008) SSDs overestimate it by about 2.5 mm. The Z_e–S relations associated with the m–D approximation from (2a) noticeably overestimate the hot-plate data. This is because this approximation provides values of the bulk density that are probably too small for larger snowflakes (Fig. 1). Note that, compared to other m–D approximations, the Z_e–S relations corresponding to (2a) provide lower values of the coefficient A in (8).

The heated tipping-bucket precipitation gauge collocated with the hot-plate sensor at the BLU site provided accumulation value, which was lower than the hot-plate result by about 30%. This value (~5 mm) was close to

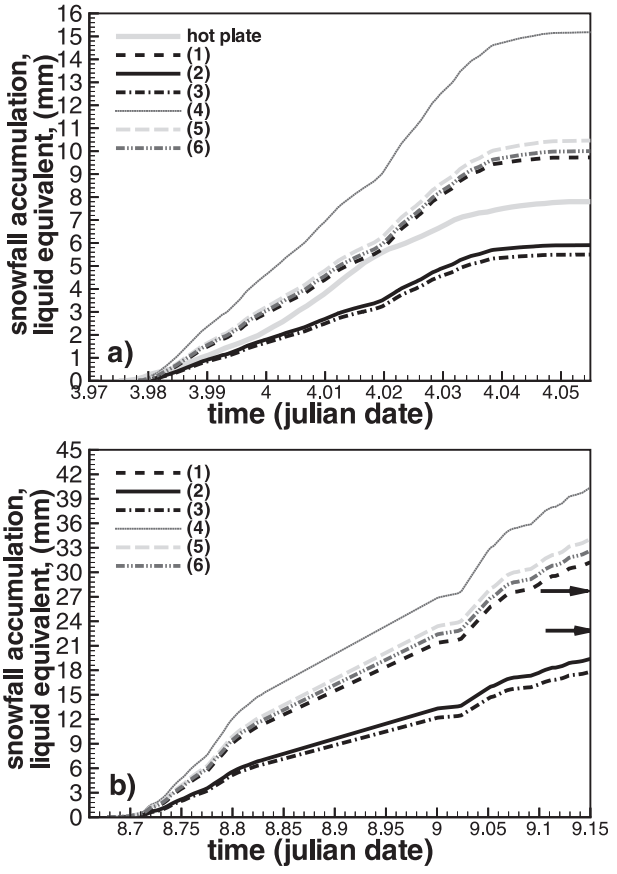

FIG. 7. Time series of snowfall accumulations as estimated from the HYDROX data at the BLU using different relations from Table 1 for the (a) 3–4 and (b) 8–9 Jan 2008 events. The upper and lower arrows in Fig. 6b show operator total accumulation estimates for the 8:1 and 10:1 snow-to-liquid ratios.

the radar data for curves (2) and (3) in Fig. 7a. Snow buildup on this gauge orifice, however, was noticed for this event; thus, its collection efficiency has been compromised. It is believed that the hot-plate sensor provided a more reliable approximation of what could be considered a "ground truth" for this observational event. Although the hot plate is not yet considered as a standard instrument, it finds a wider use in many meteorological and hydrological applications. The manufacturer (Yankee Environmental Systems) reports the accuracy of the precipitation rate measurements of ±0.5 mm h^{-1}. For events when both types of measurements were free of obvious artifacts, side-by-side comparisons of hot-plate accumulation measurements with the data from the heated bucket precipitation gauge typically indicated differences within about 15%.

A number of other ground meteorology HMT sites were located in the lower and upper parts of the North Fork ARB (see Fig. 5). All these sites, however, were at distances greater than about 17 km from the radar

location at BLU. The sites in the lower ARB were typically observing rain (or rain–snow mix) rather than dry snow, because they were located at lower altitudes. Some ground meteorology sites in the upper ARB part had tipping-bucket precipitation gauges, though the view toward them from the radar was blocked by the mountains up to beam elevations of 5.5°. Because of significant and variable vertical gradients of reflectivity in snow regions of precipitation and tipping-bucket gauge uncertainties, quantitative evaluations of the Z_e–S relation performances could be too uncertain for those remote locations, and they were not performed as part of this study.

A Particle Size and Velocity (PARSIVEL) optical disdrometer (Löffler-Mang and Blahak 2001) was collocated with other precipitation sensors at the BLU surface meteorology site. This device measures the hydrometeor size and velocity distributions in 32 size bins from 0.062 to 24.5 mm. The PARSIVEL data were available for the dry snowfall event of 3–4 January 2008. The radar reflectivity and reflectivity-weighted snowflake fall velocity (i.e., the Doppler velocity) values can generally be estimated using the PARSIVEL data and an assumption about the m–D relation (Löffler-Mang and Blahak 2001).

The working experience with the PARSIVEL disdrometer, however, indicates that SSDs derived during windy conditions ($V > 4$–5 m s^{-1}) have a significant number of artifacts resulting in unrealistic readings of snowflake fall velocities, which results in unreliable estimates of snowflake concentrations. Snowflake shape assumptions also contribute to the uncertainty of particle fall velocity estimates from PARSIVEL data. Windy conditions were common at the BLU site during the HMT-08 snowfall events; hence, reliable quantitative comparisons involving PARSIVEL estimates, which use fall velocity data, and radar measurements could not be performed. A bias in disdrometer-derived fall velocities for the event of 3–4 January 2008 is also evident from comparing the average for the whole-event vertical Doppler velocity V_D of about 1.5 m s^{-1}, as observed by the HYDROX (not shown), and the PARSIVEL estimate of this velocity, which yielded a value of about 2.1 m s^{-1} for the reflectivity-weighted mean snowflake fall velocity (i.e., the PARSIVEL estimate of V_D).

Unlike disdrometer-based snowflake concentration (and thus reflectivity) estimates, which, for a given bin size, are dependent on fall velocity measurements, the precipitation rate estimates (and thus total accumulation values), depend primarily on the integrated number of size-binned particle counts that correspond to all observed fall velocities for a given size bin and the m–D relation assumption. For the event of 3–4 January, the use

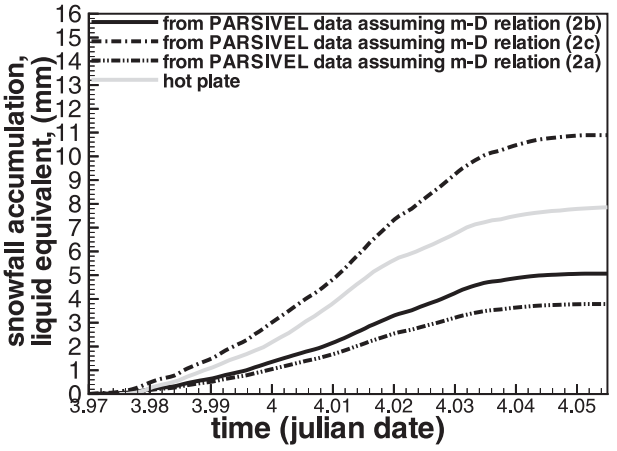

FIG. 8. Time series of snowfall accumulations as calculated from PARSIVEL SSDs and the hot-plate precipitation sensor at the BLU site for the 3–4 Jan 2008 event.

of different m–D relations with the PARSIVEL particle-count data yielded the total accumulation values of 4, 5.6, and 11 mm for relations (2a), (2b), and (2c), respectively, as shown in Fig. 8. Note that the results for the m–D relations (2c) and (2b) are within about ±35% from the hot-plate estimates, which could indicate a general appropriateness of these relations for the snowfall considered in this study.

b. An event on 8–9 January 2008

The only other prolonged dry snowfall event during the HMT-08 field deployment was observed by the HYDROX from 1600 UTC 8 January to about 0400 UTC 9 January 2008. Surface meteorology measurements during this observational event were not available because of the widespread power outage in the area, though the HYDROX operated using diesel generator power. As for the previous event, the snowflakes observed at the ground were predominantly aggregates with sizes sometimes reaching about 1 cm. Because the snow was not accumulating on the radar antenna, its performance was not compromised.

Figure 7b shows the time series of snowfall accumulation for this event calculated for the BLU site using different Z_e–S relations from Table 1. Relative differences in accumulation estimates from individual relations are similar to those observed during the previous event. At the end of this event, the radar operator took several measurements of the snow depth accumulated at the ground (snowboards) from the beginning of the radar observations. The general National Weather Service guidelines for the cooperative observers were followed during these measurements. The measurements were taken in areas free of drifting snow, and the average of these measurements was about 9 in., with a variability of

about 1 in. For snow-to-liquid ratios of 8:1–10:1 (as approximately inferred by melting the collected snow samples), the total accumulation could be estimated as about 23–28 mm. These estimates are shown in Fig. 7b by arrows. Although the 8:1 ratio may not be very representative of dry snow, the ratio 10:1 is often considered as a lower bound for such snow and is often used as an a priori value in different applications. The snow–liquid ratios mentioned before are consistent with long-term observational data of these ratios in the area of the HYDROX HMT-08 deployment (e.g., Baxter et al. 2005). Although the surface accumulation estimates are likely to have a relatively high uncertainty, they fall in the range of radar-based retrievals (Fig. 7b).

c. *Examples from previous studies*

Although dry snow X-band radar measurements during HMT deployments are scarce, some available data from previous field experiments can be used here for illustration purposes. Figure 9 shows time series of snowfall accumulations calculated using different Z_e–S relations from Table 1. The presented data correspond to aggregated dry snow conditions and come from a field experiment held near Boulder, Colorado, in 1996. During this experiment, the HYDROX was collocated with a K_a-band radar, and the main objective of the field work was to apply and verify a dual-wavelength approach for snowfall retrievals (Matrosov 1998). The snowfalls observed during this deployment were generally light to moderate and surface air temperatures were around −3° to −6°C.

It can be seen from Fig. 9 that the radar-based estimates of snowfall accumulations from the Z_e–S relations obtained with the use of surface-based Braham (1990) SSDs are in general agreement with the tipping-bucket snow gauge measurements. As during the HMT-08 deployment, the snow gauge was located in the vicinity of the radar site, and the closest useable radar range gate data were used for retrievals. The relations obtained with the aircraft-based SSDs significantly overestimate gauge data. This overestimation is more significant than for the HMT cases of heavier snowfalls shown in Fig. 7.

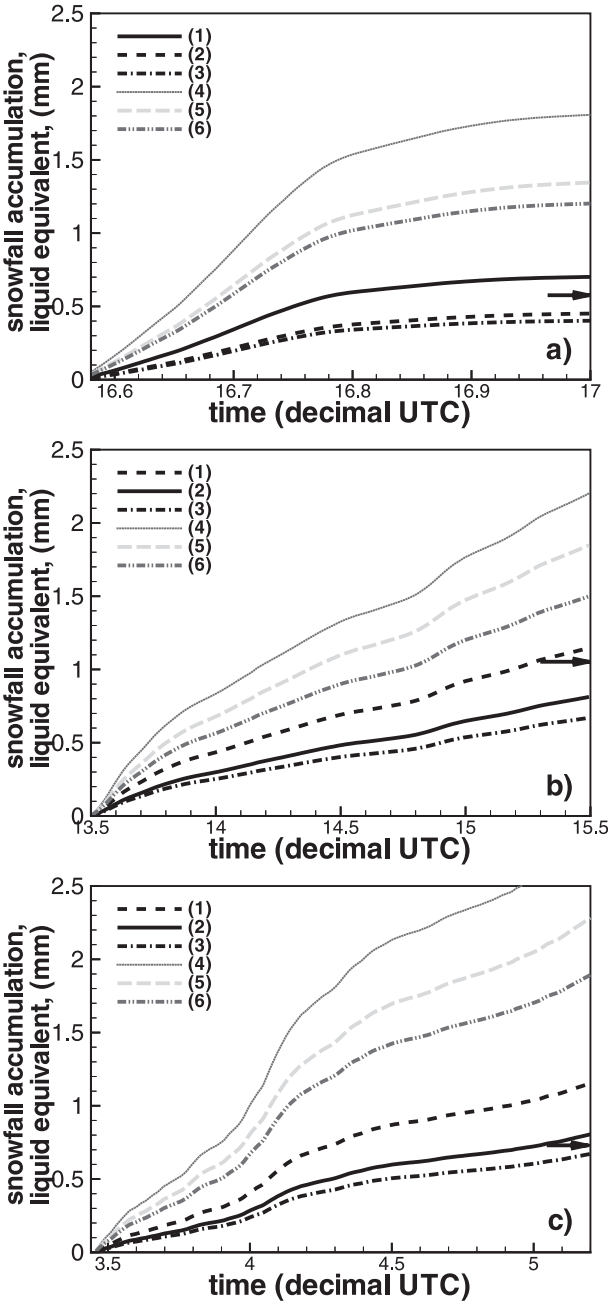

FIG. 9. Time series of snowfall accumulations as estimated from the X-band radar data near Boulder, CO, using different relations from Table 1 for (a) 22 Jan, (b) 25 Jan, and (c) 14 Mar 1996. Arrows show total accumulations from the nearby snow gauge.

5. Vertical variability of reflectivity

Section 4 comparisons of radar-derived and ground results of snowfall accumulations were performed for the estimates with small spatial separations. The height of the radar beam for these estimates was lower than 0.3–0.5 km AGL. Although the vertical variability of radar reflectivity might not be a very significant issue at scales of a few hundred meters, it becomes an important issue when radar retrievals are performed for longer ranges, where the radar beam is centered at heights located at a significant distance above the ground. In the case of stratiform rainfall, the vertical variability of reflectivity between the melting layer and the ground is usually rather small (e.g., Bellon et al. 2005) and as a rule does not exceed a few decibels. Contrary to that, at altitudes higher than the freezing level, reflectivity usually

changes with height quite significantly, which is due in part to the particle growth by vapor deposition and crystal aggregation in the snow region of precipitation.

Changes of snowfall reflectivity with height, as well as the uncertainty of these changes, present another important source of errors in radar-based estimates of snowfall at the ground when radar measurements are made at longer distances (and hence at higher altitudes). Typically, snowfall reflectivity diminishes with height with a mean gradient of about 4–5 dB km^{-1} (e.g., Matrosov and Battaglia 2009). One manifestation of this fact are the results of Hunter and Holroyd (2002), who found that, for a given radar, the most appropriate value of the coefficient A in Z_e–S relations decreases with the distance from the radar.

Several examples of the observed vertical profiles of reflectivity, which were obtained from RHI scans during the HMT-08 snowfall events of 3–4 and 8–9 January 2008, are shown in Fig. 10. In Fig. 10a, the profile observed at 2336:43 UTC 3 January 2008 [Julian day (JD) 3.984] is more or less a typical profile often observed in snow regions of precipitating systems. The mean reflectivity gradient is about 5 dB km^{-1} for this profile. The profile observed near the end of this event at 0042:26 UTC 4 January 2008 (JD 4.029) is quite different. Although at the lowest range gates both profiles yield approximately similar reflectivities, there is a much steeper reflectivity decline for the 0042:26 UTC profile up to a height of 2.5 km AGL. The upper cloud parts at around 4 km AGL, however, again exhibit similar reflectivities for both profiles. A simple vertical profile of reflectivity correction, which accounts for a mean vertical gradient of Z_e, obviously would not be generally appropriate for profiles such as the one at 0042:26 UTC.

Another illustration of vertical variability of snowfall reflectivity is shown for the event of 8–9 January 2008 in Fig. 10b. Here again, the profile observed at 1944:18 UTC 8 January (JD 8.738) is rather typical with a vertical gradient of about 4.5 dB km^{-1}. The profile at 0332:33 UTC 9 January 2008 (JD 9.148) represents a very shallow snowfall. The ground snowfall rates were, however, very similar at both times. In fact, because of this "shallowness," the last few hours of the 8–9 January 2008 event were not even detected by the Sacramento WSR-88D weather service radar (KDAX). These few hours, however, provided an appreciable accumulation at the vicinity of the BLU site.

The illustrations shown indicate the importance of the vertical profile of reflectivity as an additional uncertainty for radar-based snowfall retrievals. Retrieval errors in radar-based snowfall estimates at longer ranges resulting from vertical variability of reflectivity can be comparable or even higher than those resulting from uncertainties of snowflake properties that were assessed in this study. Detailed studies of vertical structure of snowfall reflectivity, however, is beyond the scope of this research.

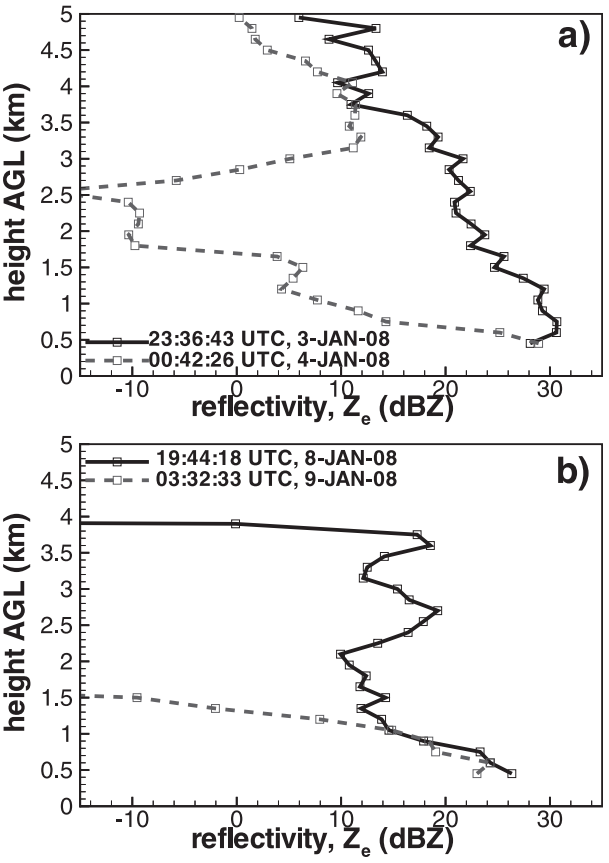

FIG. 10. Examples of vertical profiles of snowfall reflectivity observed by the HYDROX during events of (a) 3–4 and (b) 8–9 Jan 2008.

6. Summary and conclusions

Radar reflectivity–based snowfall measurements are intrinsically more uncertain than rainfall measurements. Contributing to the uncertainty is the variability in snowflake mass–size and fall velocity–size relations and in the parameters of snowflake size distributions. Shape and orientation of snowflakes also influence their backscatter properties at X-band frequencies but to a significantly lesser degree compared to the uncertainty factors mentioned earlier. This is particularly true for snowfalls with aggregate dry snowflakes, which usually result in higher precipitation rates than snowfalls consisting of single crystals. The Rayleigh assumption for calculating backscatter is typically suitable to snowflakes with sizes up to 4–5 mm. The non-Rayleigh scattering at larger snowflakes results in X-band reflectivity being smaller compared to longer wavelength radars.

Different mass–size aggregate snow particle relations found in the literature can result in almost one order of magnitude variability in calculated radar backscatter cross sections. However, the corresponding differences in the power-law relations between equivalent radar reflectivity factors and melted equivalent snowfall rates are not that great, because changes in the snowflake density influence both Z_e and S. The snowflake size distribution changes can result in about a factor of 2.5 variability in precipitation rate estimates for typical reflectivities observed in snowfall (~20–30 dBZ). Overall retrieval errors could be a factor of 2.5–3 or even higher, given other sources of uncertainty.

A set of Z_e–S relations covering a reasonable range of assumptions about snowflake densities, fall velocities, and shapes was derived for snowfall measurements at X-band radar frequencies ($\lambda \sim 3.2$ cm). For the approach used in this study, the exponential SSD parameters were adopted from different experimental studies where these parameters were estimated based on snow particle microphysical samples. Although a significant variability in the coefficients of Z_e–S relations resulting from differing assumptions was obvious, typical values of the exponent B ($Z_e = AS^B$) in these relations were in the range of 1.3–1.55. The Z_e–S relations derived using the aircraft-based experimental SSD parameters from Woods et al. (2008) have smaller values of the coefficient A (around 40) compared to the relations derived using the surface-based snow particle size spectra from Braham (1990), which produced characteristic values of A of about 100–130. The use of relations based on aircraft SSDs resulted in general overestimation of snowfall accumulations compared to ground observations. This overestimation was more significant for lighter snowfalls. The coefficient A values of about 100–120 provided the radar-based retrievals, which were in general agreement with surface estimates. Non-Rayleigh scattering effects at X band tend to diminish the coefficient A and the exponent B, compared to lower-frequency radars (e.g., S-band radars).

The derived relations were applied to experimental data observed in dry snowfalls during the wintertime field deployment of the NOAA ESRL X-band radar in the mountains of Sierra Nevada and some earlier deployments in Colorado. Although the total snowfall accumulation estimates from individual Z_e–S relations corresponding to different assumptions differed by as much as a factor of 2.5 or so (or even greater for lighter snowfalls), they bracketed accumulation estimates from the nearby ground precipitation sensors and the radar operator ground measurements. The Z_e–S relations derived with the particle mass–size relation assumptions that are usually used in ice cloud microphysical studies provided consistently higher accumulation values. The use of these relations results in the lower snow particle bulk density values compared to those obtained from studies of falling snowflakes at the ground (e.g., Holroyd 1971; Brandes et al. 2007).

Comparisons of the radar-based estimates of snowfall parameters with estimates derived from an optical disdrometer indicated a qualitative agreement between radar-derived and disdrometer estimates of snowfall accumulation values obtained using appropriate snowflake mass–size relations. The exact quantitative comparison, however, was not possible because of the relatively high uncertainties of disdrometer measurements during the HMT-08 field deployment. The radar deployment at the BLU site during HMT-08 provided only a few dry snowfall events, and the substantial areas of dry snowfall that fell in the upper parts of the basin were blocked from the radar view by the terrain. The results from HMT-08 were consistent with data obtained with the NOAA X-band radar in earlier field experiments.

More comparisons of X-band radar- and surface-based precipitation sensor measurements are needed in the future to better understand the range of applicability of the suggested Z_e–S relations and their robustness and uncertainties. Future refinements of the Z_e–S relations could use experimental SSDs derived in the HMT area from the PARSIVEL data (as they become available from disdrometer measurements) and account for temperature dependent coefficients in such relations when–if information on temperature influences on SSD and snowflake densities becomes available. The results of this study are referred to dry snowfalls with aggregate snowflakes up to 1 cm or so at negative temperatures (e.g., −10° to −1°C) with reflectivities in a range from about 24–25 to about 30–32 dBZ and differential reflectivities less than about 0.5–0.6 dB. The lack of observational data for snowfalls, where single ice crystals are the dominant particle habit, prevented exploring the applicability of the results to such snowfalls. Deriving appropriate relations for single pristine crystal snowfalls requires a special consideration.

The comparisons of radar- and ground-based measurements that were made as part of this study were performed for snowfall estimates that, if not exactly collocated, are not separated widely in space. Any use of radar-based approaches for surface snowfall estimations at longer ranges that involve interpreting radar echoes measured high above the ground also need to account for the vertical changes in snowfall reflectivity. This is an important factor to account for, because the radar reflectivity in snowfall usually exhibits clear vertical trends and diminishes with height above the ground. Given a relatively high radar-based snowfall estimation

uncertainty, one could foresee future applications when the spatial patterns of radar-derived snowfall accumulation maps are corrected for possible biases–uncertainties by the several ground-based sensors strategically located in the area of the radar coverage.

Acknowledgments. The authors are thankful to Dr. M. Stoelinga, who provided the SSD parameters from Woods et al. (2008). This study was funded by the NOAA HMT project. Many scientists and engineers from the Water Cycle branch of the ESRL's Physical Sciences division took an active part in the HMT-08 field deployment. The authors are thankful to T. Schneider (the HMT project manager), K. Clark, C. King, D. Hazen, J. Gibson, B. Bartram, and T. Ayers.

REFERENCES

Anagnostou, E. N., M. N. Anognostou, W. F. Krajewski, A. Kruger, and B. J. Mirovsky, 2004: High-resolution rainfall estimation from X-band polarimetric radar measurements. *J. Hydrometeor.,* **5,** 110–128.

Barber, P., and C. Yeh, 1975: Scattering of electromagnetic waves by arbitrarily shaped dielectric bodies. *Appl. Opt.,* **14,** 2864–2872.

Baxter, M. A., C. E. Graves, and J. T. Moore, 2005: A climatology of snow-to-liquid ratio for the contiguous United States. *Wea. Forecasting,* **20,** 729–744.

Bellon, A., G. W. Lee, and I. Zawadzki, 2005: Error statistics of VPR corrections in stratiform precipitation. *J. Appl. Meteor.,* **44,** 998–1015.

Boucher, R. J., and J. G. Wieler, 1985: Radar determination of snowfall rate and accumulation. *J. Climate Appl. Meteor.,* **24,** 68–73.

Boudala, F. S., G. A. Isaac, and D. Hudak, 2006: Ice water content and precipitation rate as a function of equivalent radar reflectivity and temperature based on in situ observations. *J. Geophys. Res.,* **111,** D11202, doi:10.1029/2005JD006499.

Braham, R. R., Jr., 1990: Snow particle size spectra in lake effects snows. *J. Appl. Meteor.,* **29,** 200–207.

Brandes, E. A., K. Ikeda, G. Zhang, M. Schönhuber, and R. M. Rasmussen, 2007: A statistical and physical description of hydrometeor distributions in Colorado snowstorms using a video disdrometer. *J. Appl. Meteor. Climatol.,* **46,** 634–650.

Brotzge, J., K. Droegemeier, and D. McLaughlin, 2006: Collaborative adaptive sensing of the atmosphere: New radar system for improving analysis and forecasting of surface weather conditions. *Trans. Res. Rec.,* **1948,** 145–151.

Brown, P. R. A., and P. N. Francis, 1995: Improved measurements of the ice water content in cirrus using a total probe. *J. Atmos. Oceanic Technol.,* **12,** 410–414.

Gunn, K. L. S., and J. S. Marshall, 1958: The distribution with size of aggregate snowflakes. *J. Meteor.,* **15,** 452–461.

Harimaya, T., H. Ishida, and K. Muramoto, 2000: Characteristics of snowflake size distributions connected with the difference of formation mechanism. *J. Meteor. Soc. Japan,* **78,** 233–239.

Heymsfield, A. J., S. Lewis, A. Bansemer, J. Iaquinta, L. M. Miloshevich, M. Kajikawa, C. Twohy, and M. R. Poellot, 2002: A general approach for deriving the properties of cirrus and stratiform ice cloud particles. *J. Atmos. Sci.,* **59,** 3–29.

Hogan, R. J., M. P. Mittermaier, and A. J. Illingworth, 2006: The retrieval of ice water content from radar reflectivity factor and temperature and its use in evaluating a mesoscale model. *J. Appl. Meteor. Climatol.,* **45,** 301–317.

Holroyd, E. W., III, 1971: The meso- and microscale structure of Great Lakes snowstorm bands: A synthesis of ground measurements, radar data, and satellite observations. Ph.D. dissertation, University at Albany, State University of New York, 148 pp.

Hunter, S. M., and E. W. Holroyd III, 2002: Demonstration of improved operational water resources management through use of better snow water equivalent information. United States Department of the Interior Bureau of Reclamation R-02-02, 75 pp.

Kingsmill, D. E., and Coauthors, 2003: TRMM common microphysics products: A tool for evaluating spaceborne precipitation retrieval algorithms. *J. Appl. Meteor.,* **43,** 1598–1618.

Korolev, A., and G. Isaac, 2003: Roundness and aspect ratio of particles in ice clouds. *J. Atmos. Sci.,* **60,** 1795–1808.

Löffler-Mang, M., and U. Blahak, 2001: Estimation of the equivalent radar reflectivity factor from measured snow size spectra. *J. Appl. Meteor.,* **40,** 843–849.

Magono, C., and T. Nakamura, 1965: Aerodynamic studies of falling snowflakes. *J. Meteor. Soc. Japan,* **43,** 139–147.

——, and C. W. Lee, 1966: Meteorological classification of natural snow crystals. *J. Fac. Sci. Hokkaido Univ.,* **2,** 321–335.

Matrosov, S. Y., 1998: A dual-wavelength radar method to measure snowfall rate. *J. Appl. Meteor.,* **37,** 1510–1521.

——, 2007: Modeling backscatter properties of snowfall at millimeter wavelengths. *J. Atmos. Sci.,* **64,** 1727–1736.

——, 2008: Assessment of radar signal attenuation caused by the melting hydrometeor layer. *IEEE Trans. Geosci. Remote Sens.,* **46,** 1039–1047.

——, and A. Battaglia, 2009: Influence of multiple scattering on CloudSat measurements in snow: A model study. *Geophys. Res. Lett.,* **36,** L12806, doi:10.1029/2009GL038704.

——, R. F. Reinking, R. A. Kropfli, B. E. Martner, and B. W. Bartram, 2001: On the use of radar depolarization ratios for estimating shapes of ice hydrometeors in winter clouds. *J. Appl. Meteor.,* **40,** 479–490.

——, K. A. Clark, B. E. Martner, and A. Tokay, 2002: X-band polarimetric radar measurements of rainfall. *J. Appl. Meteor.,* **41,** 941–952.

——, A. J. Heymsfield, and Z. Wang, 2005a: Dual-frequency radar ratio of nonspherical atmospheric hydrometeors. *Geophys. Res. Lett.,* **32,** L13816, doi:10.1029/2005GL023210.

——, D. E. Kingsnill, and F. M. Ralph, 2005b: The utility of X-band polarimetric radar for quantitative estimates of rainfall parameters. *J. Hydrometeor.,* **6,** 248–262.

——, R. F. Reinking, and I. V. Djalalova, 2005c: Inferring fall altitudes of pristine dendritic crystals from polarimetric radar data. *J. Atmos. Sci.,* **62,** 241–250.

——, K. A. Clark, and D. A. Kingsmill, 2007: A polarimetric radar approach to identify rain, melting-layer, and snow regions for applying corrections to vertical profiles of reflectivity. *J. Appl. Meteor. Climatol.,* **46,** 154–166.

Mitchell, D. L., 1996: Use of mass- and area-dimensional power laws for determining precipitation particle terminal velocities. *J. Atmos. Sci.,* **53,** 1710–1723.

——, and A. J. Heymsfield, 2005: Refinements in the treatment of ice particle terminal velocities, highlighting aggregates. *J. Atmos. Sci.,* **62,** 1637–1644.

Moisseev, D. N., and V. Chandrasekar, 2007: Examination of μ–Λ relation suggested for drop size distribution parameters. *J. Atmos. Oceanic Technol.,* **24,** 847–855.

Park, S.-G., M. Maki, K. Iwanami, V. N. Bringi, and V. Chandrasekar, 2005: Correction of radar reflectivity and differential reflectivity for rain attenuation at X band. Part II: Evaluation and application. *J. Atmos. Oceanic Technol.,* **22,** 1633–1655.

Rasmussen, R., M. Dixon, S. Vasiloff, F. Hage, S. Knight, J. Vivekanandan, and M. Xu, 2003: Snow nowcasting using a real-time correlation of radar reflectivity with snow gauge accumulation. *J. Appl. Meteor.,* **42,** 20–36.

——, and Coauthors, 2005: The hot plate snow gauge. Preprints, *13th Symp. on Meteorological Observations and Instrumentation,* Savannah, GA, Amer. Meteor. Soc., 7.3. [Available online at http://ams.confex.com/ams/pdfpapers/94403.pdf.]

Ryzhkov, A. V., T. J. Schuur, D. W. Burgess, P. L. Heinselman, S. E. Giangrande, and D. S. Zrnic, 2005: The joint polarization experiment. *Bull. Amer. Meteor. Soc.,* **86,** 809–824.

Sekhon, R. S., and R. C. Srivastava, 1970: Snow size spectra and radar reflectivity. *J. Atmos. Sci.,* **27,** 299–307.

Smith, P. L., 1984: Equivalent radar reflectivity factors for snow and ice particles. *J. Climate Appl. Meteor.,* **23,** 1258–1260.

Super, A. B., and E. W. Holroyd III, 1998: Snow Accumulation algorithm for the WSR-88D radar: Final report. United States Department of the Interior Bureau of Reclamation R-98-05, 75 pp.

Woods, C. P., M. T. Stoelinga, and J. D. Locatelli, 2008: Size spectra of snow particles measured in wintertime precipitation in the Pacific Northwest. *J. Atmos. Sci.,* **65,** 189–205.